CHEMISTRY
A EUROPEAN JOURNAL

FULL PAPER

DOI: 10.1002/chem.201202726

Manganese-Doped Highly Ordered Mesoporous Silicate with High Efficiency for Oxidation Suppression

Chang Woo Kim,[a] Minhyuk Kang,[b] Bongjin Moon,[b] Jinheung Kim,[c] and Young Soo Kang*[a]

Abstract: Herein, we demonstrate a facile approach to manganese-doped highly ordered mesoporous silicate with oxidation-suppression function. As biocompatible supports of guest ions, the ordered mesoporous silicate was synthesized by evaporation-induced self-assembly. The phase-transition from disordered to lamellar structures in the highly ordered mesoporous structure of these porosity-tuned materials was controlled by adjusting the concentration of a lab-made polystyrene-*b*-polyethylene oxide copolymer. Manganese was successfully incorporated as a guest in the hexagonally packed mesoporous silicate by using an ultrasound-assisted technique. The incorporation of manganese ions into the pores of a mesoporous silicate support could be induced for host–guest functional applications. Manganese-doped mesoporous silicate structures have been examined for their use as antioxidizing agents by electron spin resonance (ESR) measurements and radical-scavenging tests. The manganese atoms in the mesoporous structures could act in a free-radical-scavenging capacity, much like manganese nanoparticles. The high efficiency of their oxidation-suppression function is extended for application to catalytic products.

Keywords: doping · host–guest systems · manganese · mesoporous materials · radical scavengers

Introduction

Structure-directing agents (SDAs) have allowed porous materials to become promising candidates for use in applied industrial engineering because they endow these materials with many advantages, such as tunable porosity and the capability of modifying their surface characteristics by doping the surface with organic molecules.[1] Recently, porous materials were synthesized in a controlled manner by using a nanocasting technique with mesoporous silica by Vinu and co-workers and by Zhao and co-workers.[2] As a biocompatible application of porous materials, the immobilization of enzymes inside MCM-41 was first reported by Diaz and Balkus.[3] According to their study, no adsorption was observed for enzymes with molecular weights above 40 kDa because the enzyme could not be trapped inside the pores of MCM-41. Although colloidal mesoporous silicas ($mSiO_2$) have been considered to be ideal stimuli-responsive carriers for controlled-release systems, clogging of their pores with nanoparticles results in the uncontrolled attachment of a guest onto a host.[4] This research indicates that $mSiO_2$ materials with fully opened porosity are needed as hosts for biomolecules. Also, the preservation of the chemical activity of organic molecule can be enhanced by trapping the molecules inside the pores of the $mSiO_2$. For the immobilization of functional organic molecules, the pore size is a critical factor, because smaller pore sizes tend to limit the diffusion of organic molecules.[5] In addition, the suppression of bioactivity and the chemical activity of the organic molecules can be carried out by using $mSiO_2$, owing to their slow release toward the outside of their fully opened pores and their hindered structures. In particular, the antioxidant ability of the organic molecules, such as tocopherol and vitamin C, has attracted a lot of attention for applications in radical-scavenging and catalytic products. For the suppression of the degradation of such sensitive organic functional materials, antioxidizing elements, such as manganese, can be used to preserve these molecules for an extended period of time.[6]

Herein, we report the phase-transition of porosity-tuned materials by adjusting the concentration of a lab-made polystyrene-*b*-polyethylene oxide (PS-*b*-PEO) diblock-copolymer surfactant. The controlled phase-transition from disordered to lamellar structures proceeded through a hexagonally close-packed structure. In the controlled $mSiO_2$ structure, the size and shape of the pores in the hexagonally close-

[a] Dr. C. W. Kim, Prof. Y. S. Kang
Korea Center for Artificial Photosynthesis
Department of Chemistry
Sogang University
Seoul, 121-742 (Korea)
Fax: (+82) 2-701-0967
E-mail: yskang@sogang.ac.kr

[b] Dr. M. Kang, Prof. B. Moon
Department of Chemistry
Sogang University
Seoul, 121-742 (Korea)

[c] Prof J. Kim
Department of Chemistry and Nano Science
Ewha Womans University
Seoul, 120–750 (Korea)

Supporting information for this article is available on the WWW under http://dx.doi.org/10.1002/chem.201202726.

packed $mSiO_2$ material were tuned so that the pores were completely accessible to functional organic and inorganic molecules. The hexagonally close-packed $mSiO_2$ was doped with manganese ions by using an ultrasound-assisted technique and it was examined for the preservation of organic antioxidizing agents, such as vitamin C. To achieve the suppression of vitamin C, we dispersed manganese ions inside the pores of $mSiO_2$; the size of the metal particles was controlled by using various concentrations of manganese ions. In particular, the Mn-incorporated $mSiO_2$ was measured for their free-radical-scavenging and catalytic effects by room-temperature X-band electron spin resonance (ESR) spectroscopy.

Results and Discussion

As demonstrated by the pioneering work by Antonietti and co-workers, in which polybutadiene-*b*-poly(vinylpyridinium) block copolymers were used as a template to make $mSiO_2$, block-copolymer self-assembly and micro-phase separation are solvent-dependent processes.[7] Contrary to low-molecular-weight surfactants, which usually rely on water and hydrophobic effects, fully opened porosity is typically achieved by replacing the majority of the solvent by a metal or metal-oxide precursor with similar polarity and condensing this precursor around the aggregates. This process allows the synthesis of $mSiO_2$ materials with fully opened pores, which are preferable hosts for the incorporation of biomolecules and metal ions.

To control the size and shape of the $mSiO_2$ pores, a phase-transition from spherical micelles into a lamellar structure through a hexagonal close-packed mesophase was accomplished by controlling the concentration of a lab-made PS-*b*-PEO diblock polymer (Figure 1). The random thermal motion of the spherical micelles at low concentrations of the surfactants resulted in an irregular spherical shape of the porous silica, as shown in Figure 1a. As the concentration of polymer surfactant was increased, the number of spherical micelles also increased, which resulted in an increase in the order of the pores in the silica matrices. At a concentration of 0.0033 mmol of the PS-*b*-PEO diblock copolymer, highly ordered mesoporous silica was obtained, as shown in Figure 1c. Thereafter, the order in the porous silica only changed slightly, owing to the disrupted state, as shown in Figure 1d. Finally, at higher polymer-surfactant concentrations (0.0080 mmol), the phase changed into a lamellar mesophase, as shown in Figure 1e.

Figure 2a shows a SEM image along the *y* axis of the $mSiO_2$ mesophase that was obtained by hydrothermal treatment in a concentration of block-copolymer surfactant of 0.0033 mmol at 90 °C for 72 h and calcination at 650 °C for 6 h. An orthogonal view of the sample is shown in Figure 2b, which shows a highly ordered $mSiO_2$ structure. When the sample is tilted at an angle of 45° along the *x*, *y*, *z* axes, the magnified SEM and TEM images (Figure 2c,d) show a long-axis column structure along the *x*-axis and very ordered columns with a diameter of 26.6 nm. An illustration of the micelle formation by the PS-*b*-PEO diblock copolymer and hexagonally close-packed micelles of $mSiO_2$ with a pore size of 25 nm and a wall thickness of 10.8 nm is shown in the Supporting Information, Figure S1. SAXS patterns of $mSiO_2$ in 0.0033 and 0.0080 mmol solutions of the SDA are presented in the Supporting Information, Figure S2. Compared to a typical lamellar pore structure, which show indexing from the (100) and (200) planes (see the Supporting Information, Figure S2b), the Supporting Information, Figure S2a shows one first-order and two higher-order diffraction peaks from the (100), (110), and (200) planes of the mesoporous lattice, which correspond to the formation of

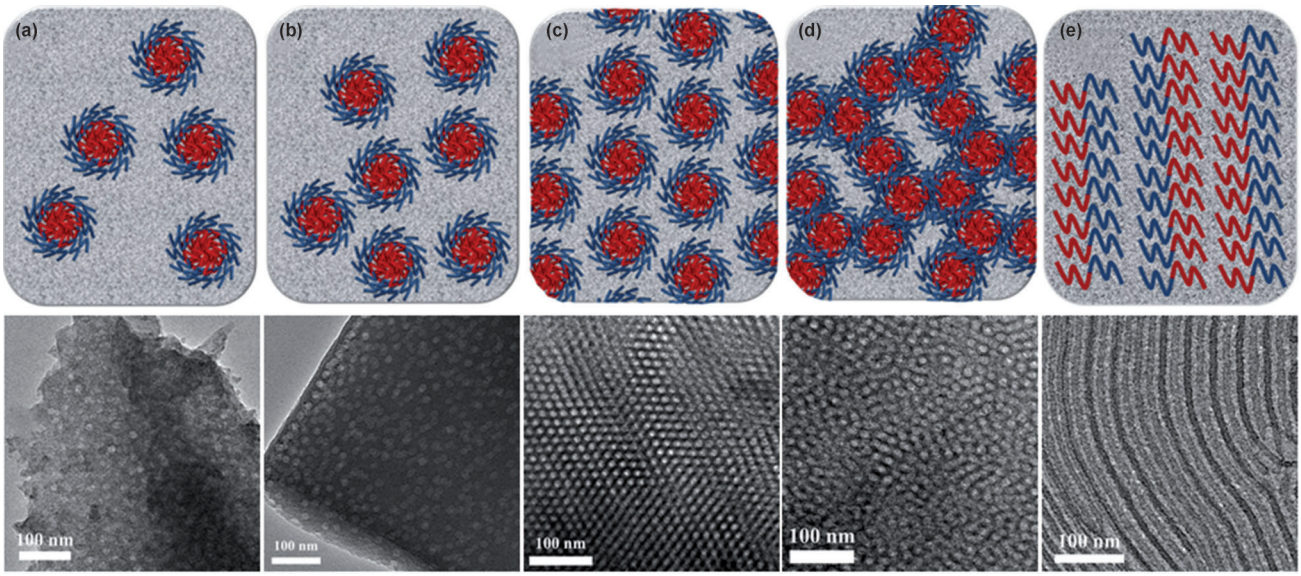

Figure 1. Phase-transition of $mSiO_2$ and TEM images of porosity-tuned $mSiO_2$, which was prepared by using different concentrations of the PS-*b*-PEO diblock copolymer: a) 0.0010 mmol, b) 0.0020 mmol, c) 0.0033 mmol, d) 0.0057 mmol, and e) 0.0080 mmol per 0.5 mL of TEOS (scale bar: 100 nm).

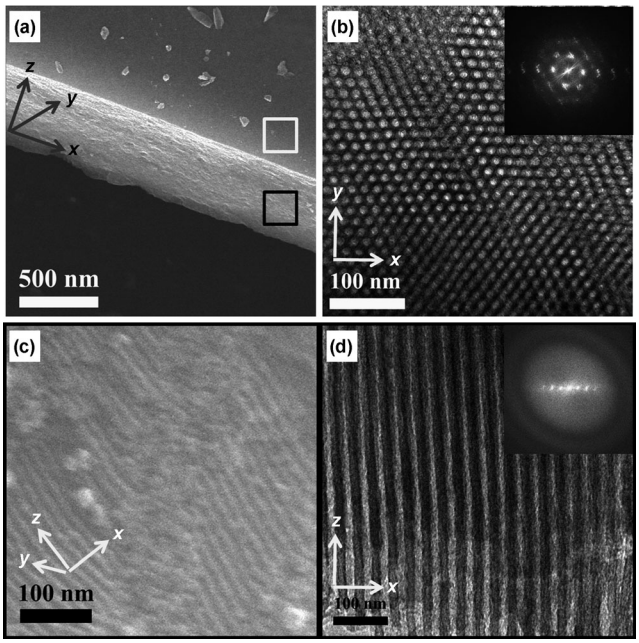

Figure 2. a) Low- and c) high-resolution SEMs and TEMs in b) the 100 plane and d) the cross-sectional 010 plane of hexagonally packed $mSiO_2$ with 0.0033 mmol of the SDA.

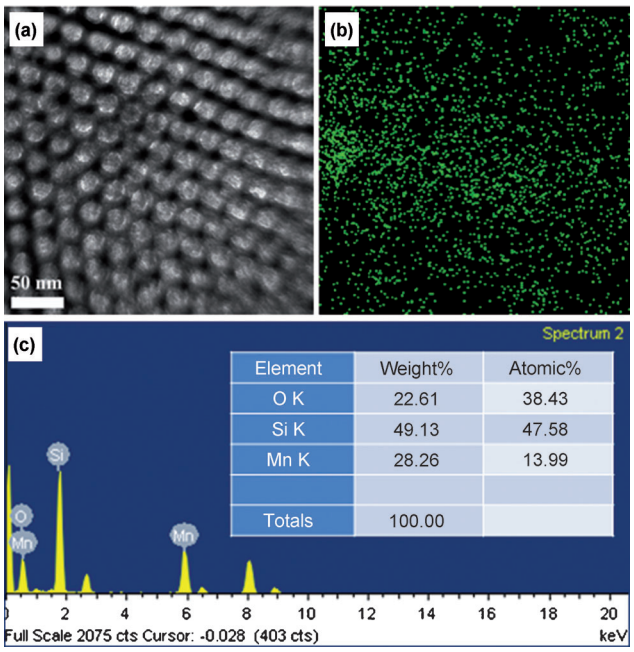

Figure 3. a) TEM image, b) Mn (green spots) elemental-mapping image, and c) EDS data of Mn-doped hexagonally packed $mSiO_2$.

hexagonally ordered pore structures. Herein, the $mSiO_2$ sample that was prepared at 0.0033 mmol of the diblock copolymer showed a surface area of 419 $m^2 g^{-1}$ and a pore diameter of 26.6 nm (determined from the BET surface area, BJH method, and SAXS measurements; see the Supporting Information, Figures S2–S4). These results show that the narrow size distribution of the pores, even with smaller diameters, could lead to a larger probability of doping organic and inorganic materials into the pores of $mSiO_2$. Compared with other mesophases, $mSiO_2$, with its hexagonal pore structure, is promising for high-temperature reactions, separation, and large-molecule catalysis.[8] The hexagonally packed $mSiO_2$ could be used as an efficient carrier of the organic antioxidizing agents by doping manganese ions. The manganese ion was doped into the pores of $mSiO_2$ by using an ultrasound-assisted technique in an aqueous solution of manganese ions.

Doping processes by using this ultrasound-assisted technique with water-soluble metal salts at an optimized concentration, reaction time, and temperature are a useful synthetic tool.[9] In our previous report, we demonstrated that metal nanoparticles were formed on the surface of SiO_2 nanoparticles through deprotonation of the hydroxy ligands, followed by the reaction of electrophilic materials, such as metal ions, at the nucleophilic sites.[9b,c] This ultrasound-assisted technique allows well-dispersed Mn ions to approach the surface of $mSiO_2$ and to attach onto partially localized surface hydroxy groups. The doping of Mn ions into the pores of $mSiO_2$ was confirmed by TEM and elemental mapping. After manganese-ion doping, the empty pores on the silica became partially blocked by the manganese ions, as shown in Figure 3.

To characterize the nature of the pores in these samples, N_2-adsorption/desorption isotherms of Mn-doped and undoped $mSiO_2$ were recorded (Figure 4a). The isotherms of Mn-doped and undoped $mSiO_2$ clearly revealed different isotherms at a relative pressure of 0.4. Whereas Mn-doped $mSiO_2$ revealed a type-II isotherm at higher relative pressures, because of its monolayer/multilayer adsorption onto the open surface of the closed pores, a type-IV isotherm (by IUPAC classification)[10] was observed for undoped $mSiO_2$. Because the type-IV isotherm for the undoped $mSiO_2$ sample is associated with capillary condensation in its mesopores, the difference between both isotherms clearly shows surface-structural differences, owing to the doping of manganese onto the surface of $mSiO_2$. Figure 4b shows high-resolution XPS spectra of Mn-doped mesoporous silicate, which shows deconvoluted Mn $2p_3$, Si $2p_3$, and O 1s signals. Taking the Fermi level as a reference ($E_f = 0$), emission bands that are related to Mn $2p_3$ in Mn-doped $mSiO_2$ should be observed at above 641.9 eV.[11] Two peaks at 642.8 and 648.0 eV are typical of a Mn 2p spectrum, owing to the $2p_{1/2}$ and $2p_{3/2}$ levels of Mn ions.[12] As-synthesized Mn-doped mesoporous silicate revealed O 1s emission with components at about 530.7 and 534.7 eV, which corresponded to the typical binding energies of oxygen in Mn–O bonds, and components at about 533.2 and 534.3 eV, which corresponded to the typical binding energies of oxygen in Si–O–Si and in Si–OH bonds. Such high-energy shifts in the binding energies of the valence electrons in the O 1s and Mn $2p_3$ orbitals are due to the formation of Mn–O and Si–O chemical bonds. Taken together, these energy-dispersive X-ray spectroscopy data, N_2-adsorption/desorption isotherms, and high-resolution XPS spectra are all consistent with the for-

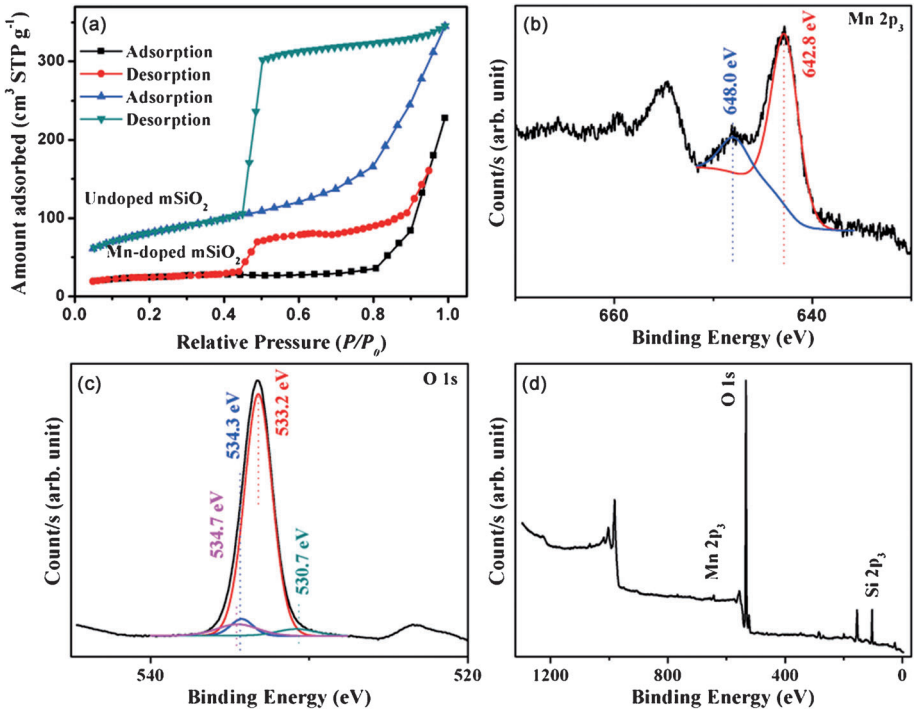

Figure 4. a) N_2-adsorption/desorption isotherms of Mn-doped and undoped $mSiO_2$. b–d) High-resolution XPS spectra of Mn-doped $mSiO_2$, which shows a Mn $2p_3$ signal, and the corresponding peak deconvolutions.

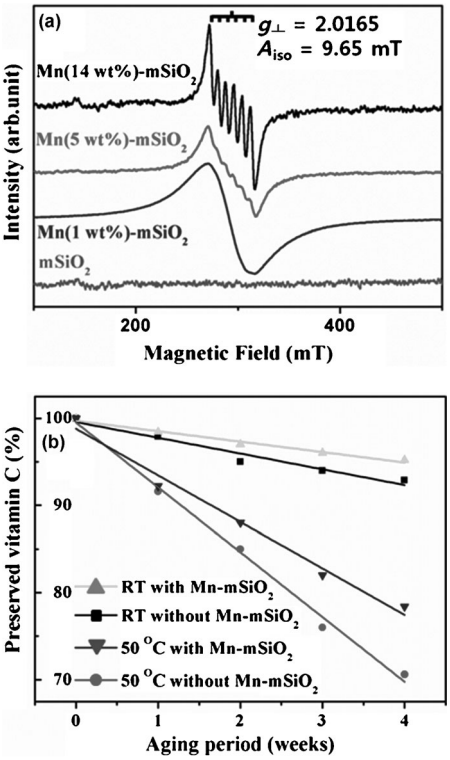

Figure 5. a) X-band ESR spectra of $mSiO_2$ and Mn-$mSiO_2$ with various Mn concentrations of 1–14 wt.% at room temperature. b) Plot of the amount of preserved vitamin C (%) of commercial cosmetics with and without Mn-$mSiO_2$ to show the effect of Mn incorporation on the suppression of the oxidation of vitamin C in the $mSiO_2$.

mation of Mn-doped $mSiO_2$, for which the relative quantity of manganese ions was determined to be 13.99 wt.%.

The homogeneous distribution of Mn ions within the pores of $mSiO_2$ is clearly shown in the elemental-mapping images, as shown in Figure 3. This result is comparable to the elemental-mapping data of Si and O in $mSiO_2$ at various manganese concentrations from 1–14 wt.% at room temperature (Figure 5a). The room-temperature ESR spectrum of Mn^{II} (14 wt.%)-doped $mSiO_2$ is shown in Figure 5a). Because Mn^{II} is well-dispersed as a paramagnetic guest throughout the $mSiO_2$ framework, a typical sextet-split ESR signal that is produced from ^{55}Mn ($I=5/2$) with a g value of 2.0165 and isotropic hyperfine coupling ($A_{iso}=$ 9.65 mT) is dominant in Figure 5a, compared with non-paramagnetic $mSiO_2$, which indicates octahedral symmetry of the Mn^{II} species. Interestingly, the broad singlet for $mSiO_2$ with 1% Mn indicated inhomogeneous aggregation on the external surface of the $mSiO_2$. Notably, this broad powder-patterned ESR signal changed into a hypersplit sextet as the concentration of Mn ions increased. Thus, that Mn ions started to become homogeneously dispersed throughout the pores of $mSiO_2$ above 1 wt.% Mn^{II}-ion concentration. This result confirms the strong hyperfine sextet ESR signal at a Mn^{II} concentration of 14 wt.%.

Based on these XPS and ESR results, the antioxidizing effect[9c,13] of manganese Mn-doped $mSiO_2$ was investigated for its application as a radical scavenger. The free-radical-scavenging capacity in Mn-doped $mSiO_2$ follows Equation (1).

$$R{-}OO^{\bullet}{+}Mn_{(x)}{+}H^{+} \rightarrow ROOH^{+}{+}Mn_{(x+1)} \quad (1)$$

To understand its free-radical-scavenging ability, the antioxidizing effects of Mn were measured as a suppression of the degradation of vitamin C (L-ascorbic acid) by free radicals. The free-radical-scavenging capacity was measured by analysis of the wt.% of preserved vitamin C. Figure 5b shows that larger amounts of vitamin C were preserved by Mn-doped $mSiO_2$ and that this preservation was aging and temperature dependent: 92.2 wt.% vitamin C was preserved after 1 week at 50°C and 78.4 wt.% was preserved after 4 weeks at 50°C. Compared with the wt.% of preserved vitamin C with un-doped $mSiO_2$, the vitamin C-preservation

efficiency improved by 7.8% after 4 weeks at 50°C with Mn-doped $mSiO_2$. This result indicates that doped manganese serves as a radical scavenger in $mSiO_2$. Notably, this functional guest element in the $mSiO_2$ holds promise for bio and catalytic applications, considering that both manganese as a guest and SiO_2 as a host are nontoxic and biocompatible materials.

Conclusion

In summary, the phase-transition of $mSiO_2$ from disordered to lamellar structures, which proceeded through a highly ordered mesophase, was achieved by controlling the concentration of a diblock copolymer. This research demonstrates that hexagonally packed $mSiO_2$ can be employed as a host for biomolecules and metal ions because of its larger pores and its highly ordered structure compared with other mesophase $mSiO_2$. In contrast to the aggregation and blocking of the mesophase pores by guest molecules in previous reports, in this case, the guest molecules were well-dispersed throughout the fully opened framework by using ultrasound treatment. Thus, the penetration of guest molecules into the pores of the $mSiO_2$ material enhanced the preservation of the chemical activity of organic molecule by trapping these molecules. In particular, the suppression of the bioactivity and chemical activity of L-ascorbic acid was achieved by using Mn-doped $mSiO_2$ with a hexagonally packed structure and completely opened pores, owing to the use of antioxidizing agents, such as Mn, to preserve the molecules of L-ascorbic acid, with their slow release toward the outside of the mesopores. This guest-doped $mSiO_2$ holds promise for applications in anti-aging or anti-wrinkling cosmetics. Moreover, this strategy could be applied to other catalytic products.

Experimental Section

Synthesis of mesoporous silicate as a support for guest ions: Poly(styrene-*block*-ethylene oxide) (PS-*b*-PEO) was synthesized according to our previously reported procedure[14] and that reported by Zhao and coworkers, with some modification.[15] The PS-*b*-PEO diblock copolymer was prepared by atom-transfer radical polymerization. An evaporation-induced self-assembly (EISA) strategy was carried out in THF by using tetraethyl orthosilicate (TEOS) as an inorganic precursor and the PS-*b*-PEO diblock copolymer as a SDA. In a typical synthesis, a desired amount of the PS-*b*-PEO diblock copolymer was stirred in THF (2.8 mL). After a clear solution was obtained, 0.1 M HCl (0.3 mL) and TEOS (0.5 mL) were added and the mixture was stirred for 20 min to form a homogeneous solution. Next, the solution was moved into glass Petri dish and then aged for 24 h. After the THF had evaporated, transparent powders were obtained on the bottom of the Petri dish. Next, the powders were hydrothermally treated in a 1.0 M solution of HCl (30 mL) at 90°C for 72 h to recrystallize the mesoporous silica framework. The silica–polymer composite was separated by centrifugation, washed with distilled water, and dried under ambient conditions. The polymer template was removed in air at 650°C for 6 h to produce the mesoporous silica.

Incorporation of manganese into the mesoporous silicate: To obtain the ability to suppress the oxidation of ascorbic acid, the concentration of doped manganese ions and their homogeneous dispersion are very important. $MnCl_2{\cdot}4H_2O$ (0.3 g) was added into a solution of EtOH and deionized water (10 mL, 7:3 v/v). Next, the previously synthesized $mSiO_2$ (0.03 g) was added into this solution and ultrasonication afforded homogeneously dispersed manganese ions inside the pores. The mixture was aged under ultrasound treatment for 30 min in an ice bath. After washing with EtOH and deionized water, the product was dried in an oven at 90°C. Ultrasound treatment was performed twice more.

Test of the antioxidizing effect of manganese towards vitamin C: Tests of the antioxidizing effect of Mn and the preparation of skin toner as a cosmetic were performed at the research center of The Face Shop Ltd. (Korea). To measure the amount of preserved vitamin C, the basic skin toner was prepared by using a basic mist, which included purified water and glycerin. Vitamin C and a desired amount of the Mn-doped mesoporous silica were added into the basic mist and the skin toner was aged for various lengths of time and at various temperatures. The skin toners with and without Mn-doped mesoporous silica were compared in terms of the wt.% of preserved vitamin C to determine their free-radical-scavenging capacity. Their wt.% of preserved vitamin C was measured by HPLC.

Characterization: Thermogravimetric analysis (TGA) was carried out on a Thermal Advantage Instrument TGA-2050 analyzer from 50–600°C under a nitrogen atmosphere or in air at a heating rate of 10°C min^{-1}. For TEM observations, the samples were prepared by placing one drop of the colloidal solution onto carbon-coated copper grids (mesh size: 200) and dried for a few minutes. The porosity of the sample was evaluated from their TEM micrographs. To determine the crystallinity and structure of the synthesized samples, Rigaku D′Max 2200 V ($Cu_{K\alpha}$ radiation, $\lambda = 1.5406$ Å) wide-angle X-ray diffraction (WAXD) and a Rigaku D′Max 2500 18 K small-angle X-ray scattering (SAXS) systems were used. Nitrogen-adsorption/desorption isotherms were measured at 77 K on an automated QUADRASORB ′SI′ analyzer (Quantachrome Instruments). High-resolution X-ray photoelectron spectroscopy (XPS) spectra of Mn-doped mesoporous silicate were recorded on an X-ray photoelectron spectrometer (THERMO VG SCIENTIFIC, MultiLab2000) at Pukyong National University, Korea. ESR spectra of $mSiO_2$ with various manganese content were recorded on a JEOL (Japan) JES PX 2300 FT-ESR with a 1.4 T electromagnet and an output frequency of 8800–9600 MHz (X-band) at Pukyong National University, Korea.

Acknowledgements

This work was supported by the Basic Science Research Program through the National Research Foundation of Korea (NRF) and by a grant from the Ministry of Education, Science and Technology of Korea (MEST) for the Center for Next Generation Dye-sensitized Solar Cells (No. 2012–0000591).

[1] a) N. Linares, E. Serrano, M. Rico, A. M. Balu, E. Losada, R. Luque, J. Garcıa-Martınez, *Chem. Commun.* **2011**, *47*, 9024; b) S.-H. Wu, Y. Hung, C.-Y. Mou, *Chem. Commun.* **2011**, *47*, 9972; c) P. Wu, Z. Xiong, K. P. Loh, X. S. Zhao, *Catal. Sci. Technol.* **2011**, *1*, 285; d) A. Vinu, V, Murgesan, O. Tangermann, M. Hartmann, *Chem. Mater.* **2004**, *16*, 3056; e) M. Vallet-Regí, F. Balas, D, Arcos, *Angew. Chem.* **2007**, *119*, 7692; *Angew. Chem. Int. Ed.* **2007**, *46*, 7548.

[2] a) E. Haque, J. W. Jun, S. N. Talapaneni, A. Vinu, S. H. Jhung, *J. Mater. Chem.* **2010**, *20*, 10801; b) L.-C. Sang, A. Vinu, M.-O. Coppens, *J. Mater. Chem.* **2011**, *21*, 7410; c) Z. Zhou, Q. Yan, F. Su, X. S. Zhao, *J. Mater. Chem.* **2005**, *15*, 2569.

[3] a) J. F. Díaz, K. J. Balkus, *J. Mol. Catal. B* **1996**, *2*, 115; b) M. E. Gimon-Kinsel, V. L. Jimenez, L. Washmon, K. J. Balkus, *Stud. Surf. Sci. Catal.* **1998**, *117*, 373.

[4] a) Z. Luo, K. Cai, Y. Hu, L. Zhao, P. Liu, L. Duan, W. Yang, *Angew. Chem.* **2011**, *123*, 666; *Angew. Chem. Int. Ed.* **2011**, *50*, 640; b) A. Schlossbauer, S. Warncke, P. M. E. Gramlich, J. Kecht, A. Manetto,

T. Carell, T. Bein, *Angew. Chem.* **2010**, *122*, 4842; *Angew. Chem. Int. Ed.* **2010**, *49*, 4734; c) S. Liu, H. Chen, X. Lu, C. Deng, X. Zhang, P. Yang, *Angew. Chem.* **2010**, *122*, 7719; *Angew. Chem. Int. Ed.* **2010**, *49*, 7557.
[5] A. Vinu, M. Miyahara, V. Sivamurugan, T. Morib, K. Ariga, *J. Mater. Chem.* **2005**, *15*, 5122.
[6] a) L. Gómez-Hortiguela, F. Cora, C. R. A. Catlow, *ACS Catal.* **2011**, *1*, 18; b) M. Oba, Y. Oaki, H, Imai, *Adv. Funct. Mater.* **2010**, *20*, 4279; c) C. Yu, L. Zhang, J. Shi, J. Zhao, J. Gao, D. Yan, *Adv. Funct. Mater.* **2008**, *18*, 1544.
[7] a) E. Krämer, S. Forster, C. Goltner, M. Antonietti, *Langmuir* **1998**, *14*, 2027; b) B. Smarsly, M. Antonietti, *Eur. J. Inorg. Chem.* **2006**, *6*, 1111.
[8] X. Dong, W. Shen, Y. Zhu, L. Xiong, J. Shi, *Adv. Funct. Mater.* **2005**, *15*, 955.
[9] a) G. R. Patzke, Y. Zhou, R. Kontic, F. Conrad, *Angew. Chem.* **2011**, *123*, 852; *Angew. Chem. Int. Ed.* **2011**, *50*, 826; b) Y. H. Kim, D. K. Lee, H. G. Cha, C. W. Kim, Y. C. Kang, Y. S. Kang, *J. Phys. Chem. B* **2006**, *110*, 24923; c) C. W. Kim, U. Pal, S. Park, J. Kim, Y. S. Kang, *Chem. Eur. J.* **2012**, *18*, 12314.
[10] a) K. S. W. Sing, D. H. Everett, R. A. W. Haul, L. Moscou, R. A. Pierotty, J. Rouquerol, T. Siemieniewska, *Pure Appl. Chem.* **1985**, *57*, 603; b) X. S. Zhao, F. Su, Q. Yan, W. Guo, X. Y. Bao, L. Lv, Z. Zhou, *J. Mater. Chem.* **2006**, *16*, 637.
[11] B. V. Crist, Handbook of Monocromatic XPS Spectra: The Elements and Native Oxides, John Willey and Sons Ltd, Chichester, **2000**, pp. 165–168.
[12] R. Silvio, J. Rubio, *Mineals Engineering.* **2010**, *23*, 1131.
[13] M. Coassin, F. Ursini, A. Bindoli, *Archives of Biochemistry and Biophysics.* **1992**, 299, 330.
[14] M. Kang, B. Moon, *Macromolecules* **2009**, *42*, 455.
[15] Y. Deng, T. Yu, Y. Wan, Y. Shi, Y. Meng, D. Gu, L. Zhang, Y. Huang, C. Liu, X. Wu, D. Zhao, *J. Am. Chem. Soc.* **2007**, *129*, 1690.

Received: July 30, 2012
Published online: November 22, 2012

